Engineering Structures 72 (2014) 113–122

Contents lists available at ScienceDirect

Engineering Structures

journal homepage: www.elsevier.com/locate/engstruct

Simple and efficient finite element modeling of reinforced concrete columns confined with fiber-reinforced polymers

D. Hu, M. Barbato *

Engineering Corporation of Louisiana, Lafayette, LA, United States
Civil and Environmental Engineering, Louisiana State University and A&M College, Baton Rouge, LA, United States

ARTICLE INFO

Article history:
Received 26 January 2014
Revised 26 March 2014
Accepted 16 April 2014

Keywords:
Fiber-reinforced polymer composites
Reinforced concrete
Confinement
Nonlinear material behavior
Finite element method

ABSTRACT

This paper presents a frame finite element (FE) that is able to accurately estimate the load-carrying capacity and ductility of reinforced concrete (RC) circular columns confined with externally-bonded fiber-reinforced polymers (FRP). This frame FE can model collapse mechanisms due to concrete crushing, reinforcement steel yielding, and FRP rupture. The adopted FE considers distributed plasticity with fiber discretization of the cross-sections in the context of a force-based formulation, and uses advanced nonlinear material constitutive models for reinforcing steel and unconfined, steel-confined, and FRP-confined concrete.

The adopted frame FE is validated through a comparison between numerical simulations and experimental results available in the literature of the load-carrying capacity of FRP-confined RC columns subjected to axial load only, and both axial and lateral load. The adopted FE is suitable for efficient and accurate modeling and analysis of FRP-confined RC columns, and thus it represents a step toward enabling analysis of real-world large-scale structures containing FRP-confined RC columns, for which more accurate three-dimensional models could be computationally prohibitive.

1. Introduction

Externally-bonded fiber-reinforced polymer (FRP) composites have found numerous applications in civil engineering structures due to their high strength-to-weight and stiffness-to-weight ratios, corrosion resistance, and high durability [1,2]. One of these applications is the FRP confinement of reinforced concrete (RC) columns to improve their structural performance in terms of ultimate load bearing capacity and ductility [3,4]. The FRP confinement of RC columns presents numerous advantages compared to other rehabilitation techniques, e.g., RC section enlargement and confinement using steel jackets. Some of these advantages include negligible increase in structural size and weight, easy transportation, and good resistance to corrosion and other degradation processes due to harsh environmental conditions [5]. This method has been widely used to retrofit bridges and buildings in the past two decades [6–8]. The proper use of this rehabilitation procedure requires the accurate prediction of the improved performance of the FRP-confined RC columns based on the specific geometry, material properties, and amount of FRP utilized. Numerous numerical tools have been developed to model the structural behavior of FRP-confined RC columns. These tools include (1) stress–strain models of FRP-confined concrete at the material level, (2) stress resultant-section deformation relations at the cross-section level, and (3) finite element (FE) models of structural components at the structural level.

Extensive studies available in the literature have been conducted to develop appropriate stress–strain relations for FRP-confined concrete. These stress–strain models can be classified into two categories: design-oriented and analysis-oriented models [9]. Design-oriented models [10–14] provide closed-form equations directly calibrated on experimental results for predicting the compressive strength, ultimate axial strain, and stress–strain behavior of FRP-confined concrete; whereas analysis-oriented models [15–18] derive stress–strain curves that are generated using incremental numerical procedures typically used within nonlinear FE models. A few models for sectional analysis of FRP-confined RC columns have been developed in the last decade. In [19], a fiber-section model was used to discretize the cross-section into fibers of unconfined concrete, confined concrete, steel rebars, and confining FRP. The structural force–deformation relation was derived by numerical integration of the stress–strain relation of the fibers at the column base section. In [20], a two-dimensional sectional analysis of RC columns confined with FRP was presented, in which the bending moment strength was determined through analytical

* Corresponding author.
E-mail addresses: danh@ecl-eng.com (D. Hu), mbarbato@lsu.edu (M. Barbato).

http://dx.doi.org/10.1016/j.engstruct.2014.04.033
0141-0296/

integration of the stresses corresponding to material constitutive models used for design. The FE method has been widely used as a powerful tool to effectively model the behavior of FRP-confined RC columns. A significant number of previous FE studies employed refined FE meshes of three-dimensional solid elements using commercially available software, such as ANSYS [21], ABAQUS [22,23], and MARC™ [24], or research software such as DYNA3D [25], and FEMIX [26]. The computational cost of similar structural response analyses is usually extremely high, because of the large number of elements and degrees of freedom involved, and the need to use three-dimensional constitutive models for all materials considered in the FE analyses. In [27], appropriate material constitutive models were implemented in the framework of fiber-discretized frame elements using a displacement-based formulation. This computational model employed a variable confinement relation based on a non-uniform confinement distribution in the compression zone.

The efficient modeling of the structural behavior of FRP-confined RC columns through the FE method remains an active research field, due to the difficulties in understanding and predicting the complex interaction between confined and unconfined concrete, reinforcing steel, and confining FRP. The validation and calibration of FE models is made even more complex by the high cost and difficulties of producing test data from FRP-confined RC columns. The contribution of this study is the combination and implementation of existing modeling tools (i.e., force-based formulation for frame elements, fiber discretization of the cross-sections, and existing advanced material constitutive models for concrete and reinforcing steel) into a nonlinear frame FE that enables one to model the mechanical behavior of FRP-confined RC columns in an accurate and computationally efficient fashion, and that can be used for a computationally feasible nonlinear FE analysis of entire real-world structures, e.g., bridges subject to seismic excitation, for which more accurate three-dimensional models could be computationally prohibitive. To the authors' knowledge, this study employs for the first time a force-based frame FE with fiber-discretized cross-sections to model the structural response of FRP-confined RC columns. This paper focuses on RC columns with circular cross-section confined by externally-bonded FRP with fibers oriented along the hoop direction (i.e., orthogonal to the axis) of the columns.

2. Finite element modeling

2.1. Finite element formulation

This study adopted a two-node one-dimensional force-based frame FE [28] with Euler–Bernoulli kinematic assumptions under small deformations and small displacements (i.e., linear geometry) to model the structural response of FRP-confined RC columns. A fiber discretization was employed to evaluate the cross-section nonlinear behavior [28]. Realistic one-dimensional nonlinear constitutive models were employed to describe the stress–strain behavior of unconfined, steel-confined, and FRP-confined concrete, as well as of reinforcing steel. In this study, the element state determination was based on the non-iterative algorithm [29], whereas the integrals in the element formulation were evaluated numerically following a Gauss–Lobatto (G–L) integration scheme with a user-defined number of integration points (i.e., monitored cross-sections). It is noteworthy that other element state determination algorithms (e.g., the iterative algorithm proposed in [28]) and numerical integration schemes (e.g., Gauss–Legendre integration) can be also used in conjunction with the frame FE element developed in this study.

The outstanding features of the adopted frame FE include computational efficiency, high accuracy even when a coarse FE mesh is used, and ease of use. The computational efficiency of this frame element derives from the use of (1) the force-based formulation, which for frames imposes equilibrium exactly along the element axis and reduces the number of elements needed for an appropriate mesh of the FE model when compared to a displacement-based formulation [28,29]; and (2) the cross-section fiber discretization that allows the structural analyst to use one-dimensional material constitutive models only, which are computationally less demanding than their three-dimensional counterparts [28]. The accuracy of the adopted frame FE derives from the capability of the fiber-section models to closely represent the nonlinear interaction between axial forces and bending moments at the cross-section level, and the high fidelity of the one-dimensional material constitutive models in describing the actual stress–strain relations for the different materials used in FRP-confined RC columns. The ease of use of this frame FE is due to the fact that FE models built by using force-based frame elements are virtually mesh-independent, in the sense that the same mesh discretization can be used for linear and nonlinear FE analysis while equilibrium is enforced exactly along all members [28].

2.2. Material modeling and computation of cross-section stress resultants

In the adopted FE, the cross-section stress resultants (axial force and bending moment) are computed using a fiber discretization of the circular cross-section [19], as shown in Fig. 1. The concrete fibers are defined through a radial discretization (defined by parameters R_i = internal radius, R_e = external radius, R_c = confined radius, n_{r1} = number of steel-confined radial layers, and n_{r2} = number of unconfined radial layers) and an angular discretization (defined by parameters θ_i = initial angle, θ_e = end angle, and n_a = number of angular subdivision) of the cross-section. In addition, each reinforcing steel rebar corresponds to an additional fiber, which is described by the parameters A_{b_i} = area of the ith steel rebar, θ_{b_i} = angle for the ith steel rebar, and R_{b_i} = radius at which the ith steel rebar is located (with $i = 1, 2, \ldots, n_b$, n_b = number of reinforcing steel bars). The nonlinear stress–strain response of each discretization fiber is described by appropriate one-dimensional nonlinear material constitutive models.

The constitutive behavior of the steel reinforcement was modeled using the one-dimensional Menegotto-Pinto plasticity model

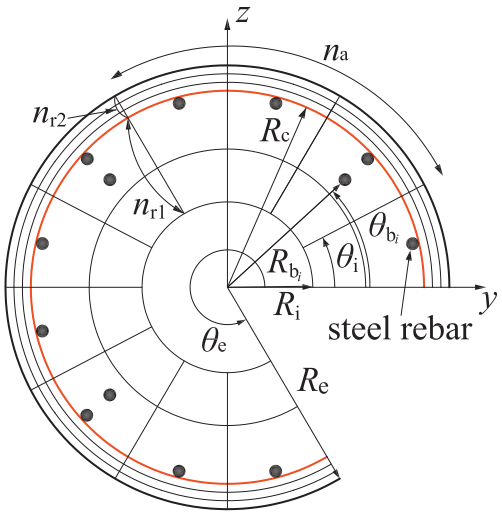

Fig. 1. Fiber discretization of a circular cross-section.

[30] as extended in [31] to account for isotropic strain hardening and in [32] to account for local buckling of steel rebars. This model is a computationally efficient smooth inelastic model typically used for structural steel, which showed very good agreement with experimental results of steel rebars. The constitutive law for the unconfined concrete material was a uniaxial cyclic law with a monotonic envelope given by the Popovics-Saenz law [32–35]. The well-known Mander model was employed in this study to describe the behavior of concrete confined by steel [36]. In order to investigate the effects of using different material models on the numerical response of FRP-confined RC columns, two material constitutive models of FRP-confined concrete were adopted and conveniently modified, namely the Spoelstra-Monti model [16] (referred to as SM model hereinafter) and the Shao-Zhu-Mirmiran model [18] (referred to as SZM model hereinafter). These two material constitutive models were selected because they have a well-defined set of rules for cyclic response (see [37] for the SM model and [18] for the SZM model), which makes them ideal for implementation within a general-purpose FE program. The SM model is based on an incremental-iterative scheme that explicitly accounts through equilibrium for the interaction between concrete and confining FRP due to the concrete lateral strain. This model can trace the strain state in the FRP and detect its failure. The SZM model is a stress–strain relation parameterized with respect to the mechanical and geometric properties of the FRP confinement. This parameterized stress–strain curve was obtained through fitting of extensive experimental tests on FRP-confined concrete cylinders [12]. Zero strength and stiffness in tension are assumed here for all concrete constitutive models. It is noted here that the failure strain of the confining FRP is an input parameter for both SM and SZM models, which significantly affects the estimates of the peak strength and of the axial strain at peak strength for the confined concrete. It is also known that, in general, the hoop rupture stress is smaller than the failure stress measured on flat FRP coupons [9,38]. Thus, for accurate prediction of the structural behavior of FRP-retrofitted RC columns, the hoop rupture stress needs to be estimated, e.g., by using appropriate models for the FRP efficiency factor [9,38,39] or by directly measuring the hoop rupture stress/strain [40]. Typical monotonic stress–strain relationships of these constitutive models are shown in Fig. 2 (in which f'_{co} = unconfined compressive concrete strength, E_s = steel Young's modulus, E_f = FRP Young's modulus, f_{yh} = yield strength of confining steel, ρ_s = volumetric steel ratio, and ρ_f = volumetric FRP ratio).

This study focuses on columns with circular cross-section, since the adopted material constitutive models for the FRP-confined concrete were developed for uniform confinement conditions [16,18].

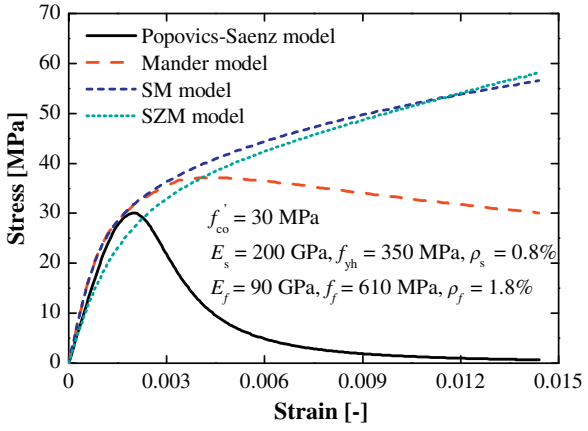

Fig. 2. Monotonic stress–strain responses of constitutive material models for unconfined, steel-confined, and FRP-confined concrete.

The adoption of the SM and SZM models is justified by the use of a fiber-discretization of the cross-sections, which imposes that each fiber is subjected to only axial strains and stresses that are assumed constant over the entire fiber and equal to their values at the fiber center point. Under these assumptions, each fiber is in a condition of uniform confinement even when the entire cross-section is under a condition of non-uniform confinement, e.g., for combined axial and transversal loading conditions. It is noteworthy that FRP confinement is a contact-critical application for externally-bonded FRP [38]. Thus, interface debonding does not affect significantly the mechanical behavior of FRP-confined RC columns with fibers oriented only in the hoop direction (as those considered in this study) and is not a significant concern in their FE modeling.

2.3. Computer implementation

The adopted frame FE for nonlinear FE response analysis of RC columns confined with externally-bonded FRP was implemented in FEDEASLab [41], a Matlab-based [42] program suitable for linear and nonlinear, static and dynamic structural analysis. FEDEASLab contains several different options for load and time stepping schemes, as well as for iterative schemes used to solve systems of nonlinear equations. By taking advantage of the modularity of FEDEASLab, the existing element, section, and material libraries were extended (i.e., 6-degrees-of-freedom force-based RC column element confined with FRP, circular fiber-discretized cross-section with FRP confinement, SM and SZM constitutive models for FRP-confined concrete) to enable accurate modeling and response simulation of FRP-confined RC columns. These FE libraries can be easily updated and/or extended to reflect the state-of-the-art in modeling such structures, since each analysis component at element, section, and material is independent of the other components (e.g., the material constitutive models can be modified or substituted with other material models without the need to modify the element model and the section model, or the formulation of the frame FE can be modified without affecting the material constitutive models and the section model). It is also noteworthy that, since the main goals of this paper are the description and validation of the extension of the adopted frame FE to analysis of FRP-confined RC columns, the application examples presented here are very simple (i.e., monotonically loaded cantilever columns) and other techniques simpler than FE analysis can be used to analyze them (e.g., direct integration of the local moment–curvature relationships). However, as currently implemented in FEDEASLab, this frame FE can be used for nonlinear static and dynamic FE analyses of real-world structural systems.

3. Correlation between numerical simulation and experimental results

The adopted FE was validated through a detailed comparison of experimentally recorded and numerically simulated response results corresponding to a significant number of FRP-retrofitted circular columns with a static scheme corresponding to a cantilever structure and subjected to two different quasi-static loading conditions. The loading conditions considered in this study are referred to as (1) concentric axial loading, which corresponds to the application of a monotonically increasing axial deformation, and (2) eccentric axial loading, which corresponds to the application of a monotonically increasing transversal deformation at the free end of the cantilever under a constant axial load. A careful literature study was completed in order to collect the experimental data used here. The publications from which the response experimental data were taken also contained a description of the column

specimens' geometry and material properties, which was sufficiently detailed to build the corresponding FE model. The description of the selected experimental column specimens, as well as the references from which the data were taken, is provided in Table 1 for the columns subjected to concentric axial loading, and in Table 2 for the columns subjected to eccentric axial loading. For the concentric axial loading case, this study considered a set of 37 RC columns, of which nine were control specimens (without FRP retrofit) and 28 were RC columns confined using externally-bonded FRP. For the eccentric axial loading case, this study considered a set of 19 RC columns, of which six were control specimens (without FRP retrofit) and 13 were RC columns confined using externally-bonded FRP. All FE analyses performed in this study are quasi-static nonlinear analyses based on an incremental displacement-controlled technique and the Newton–Raphson iterative procedure [43].

3.1. Finite element model convergence study

A convergence analysis study was performed to determine an appropriate FE mesh and cross-section discretization to be used in the comparison between experimental and numerical results. This convergence analysis study considered the following ranges of modeling parameters: (1) $n_{FE} = 1, 2, 3$ (where n_{FE} = number of FEs); (2) $n_{GL} = 3, 5, 10$ (where n_{GL} = number of G–L integration points); (3) $n_{r1} = 20, 40$; and (4) $n_a = 20, 40$. The number of unconfined radial layers was kept constant and equal to $n_{r2} = 10$. The computational cost of each FE analysis increases proportionally to the increasing resolution of the FE mesh and cross-section discretization. Thus, it is useful to find the FE mesh and cross-section discretization with the smallest resolution for which the FE response results are converged within a given (user-defined) tolerance.

The results of the convergence analysis are reported here for the column specimen identified as ST3NT in [44]. The ST3NT specimen consisted of a column with diameter $d = 356$ mm and a shear span length $L = 1470$ mm, cast integrally with a $510 \times 760 \times 810$ mm stub. The relevant geometric and material properties for the specimen were taken from [44] and are reported in Table 2. The column was tested under eccentric axial loading. Fig. 3 provides the moment–curvature response results computed at the fixed end section using FE models with different meshes and cross-section discretizations. The inset of Fig. 3 represents a zoom view of the moment–curvature curve, which shows that response convergence is practically achieved for the FE model with one FE, 5 G-L integration points, 20 radial layers, and 20 angular subdivisions. This convergence analysis was repeated for several specimens with and without FRP retrofit, subjected to both concentric and eccentric axial loading. In all cases considered, the FE response was already practically converged using $n_{FE} = 1$, $n_{GL} = 5$, $n_{r1} = 20$, and $n_a = 20$. Thus, in the remainder of this paper, for all specimens with constant cross-section properties along their length, a FE model with a single FE mesh and five G–L integration points was adopted. All cross-sections were discretized using 20 steel-confined radial layers and 20 angular subdivisions.

Table 1
Experimental test database for RC columns subjected to concentric axial loading.

Ref.	ID	d (mm)	L (mm)	f'_{co} (MPa)	n_b (–)	A_b (mm^2)	f_y (MPa)	FRP type	t_f(mm)	E_f (GPa)	f_j (MPa)
[45]	C01-L0-20	356	1524	29.8	6	300	402	CFRP	1	41.2	885
	C01-L0-26	356	1524	29.8	6	300	402	CFRP	2	41.2	885
[46]	00-LS320-3	356	1524	29.8	6	300	402	–	–	–	–
	G01-L0-9	356	1524	29.8	6	300	402	GFRP	1	22.6	535
	G01-L0-13	356	1524	29.8	6	300	402	GFRP	2	22.6	535
[47]	C1	508	1830	26.2	8	380	450	–	–	–	–
	C2	508	1830	26.2	8	380	450	GFRP	3	19.1	330
	C3	508	1830	26.2	8	380	450	GFRP	3	21.6	383
	C4	508	1830	26.2	8	380	450	CFRP	3	38.1	580
[48]	K1	400	2000	31.8	10	113	620	–	–	–	–
	K2	400	2000	34.3	10	113	620	CFRP	0.585	198	2600
	K3	400	2000	34.3	10	113	620	CFRP	0.94	480	1100
	K4	400	2000	39.3	10	113	620	GFRP	1.8	60	780
	K5	400	2000	39.3	10	113	620	GFRP	0.6	60	780
	K8	400	2000	39.1	10	113	620	HFRP	0.492	120	1100
[49]	A5NP2C	303	1200	29.4	6	201	423	CFRP	0.762	78	1050
	C4NP0C	303	1200	31.7	6	201	423	–	–	–	–
	C4NP2C	303	1200	31.7	6	201	423	CFRP	0.762	78	1050
	C4NP4C	303	1200	31.7	6	201	423	CFRP	1.524	78	1050
	B4NP2C	303	1200	31.7	6	201	550	CFRP	0.762	78	1050
	C4MP0C	303	1200	50.8	6	201	423	-	-	-	-
	C4MP2C	303	1200	50.8	6	201	423	CFRP	0.762	78	1050
[50]	I.RCC.0L	160	320	25.93	4	113	500	–	–	–	–
	I.RCC.1L	160	320	25.93	4	113	500	CFRP	1	34	450
	I.RCC.3L	160	320	25.93	4	113	500	CFRP	3	34	450
	II.RCC.0L	160	320	49.46	4	113	500	–	–	–	–
	II.RCC.1L	160	320	49.46	4	113	500	CFRP	1	34	450
	II.RCC.3L	160	320	49.46	4	113	500	CFRP	3	34	450
	III.RCC.0L	160	320	61.81	4	113	500	–	–	–	–
	III.RCC.1L	160	320	61.81	4	113	500	CFRP	1	34	450
	III.RCC.3L	160	320	61.81	4	113	500	CFRP	3	34	450
[51]	C10	150	750	38	6	28	391	CFRP	0.334	226	3339
	C30	250	750	35.2	6	113	458	–	–	–	–
	C41	250	750	35.2	6	113	458	CFRP	0.176	241	3937
	C34	250	750	35.2	6	113	458	CFRP	0.352	241	3937
	C43	250	750	35.2	6	113	458	CFRP	0.528	241	3937
	C44	250	750	35.2	6	113	458	CFRP	0.704	241	3937

Table 2
Experimental test database for RC columns subjected to eccentric axial loading.

Ref.	ID	d (mm)	L (mm)	f'_{co}(MPa)	n_b (–)	A_b (mm^2)	f_y (MPa)	FRPType	t_f (mm)	E_f (GPa)	f_j (MPa)
[54]	As-built	305	1892	34.5	9	201	358	–	–	–	–
	Upgraded	305	1892	34.5	9	201	358	GFRP	4.8	18.6	532
[4]	As-built	610	3658	34.45	26	284	303	–	–	–	–
	#1	610	3658	34.45	26	284	303	CFRP	5.1	124	1300
	#2	610	3658	34.45	26	284	303	CFRP	6.3	124	1300
[44]	S-2NT	356	1470	40.1	6	500	450	–	–	–	–
	S-3NT	356	1470	39.2	6	500	450	–	–	–	–
	S-4NT	356	1470	39.2	6	500	450	–	–	–	–
	ST-2NT	356	1470	40.4	6	500	450	GFRP	1.25	20	400
	ST-3NT	356	1470	40.4	6	500	450	CFRP	1.00	20	900
	ST-4NT	356	1470	44.8	6	500	450	CFRP	0.50	75	900
	ST-5NT	356	1470	40.8	6	500	450	GFRP	1.25	20	400
[55]	BR-C8	508	2000	38	12	302	400	–	–	–	–
	BR-C8-1	508	2000	38	12	302	400	CFRP	3.6	60	700
	BR-C8-2	508	2000	38	12	302	400	CFRP	1.8	60	700
[56]	RC-1	270	2000	90.1	8	201	500	CFRP	0.66	227	3800
	RC-2	270	2000	75.2	8	201	500	CFRP	0.33	227	3800
	RC-3	270	2000	49.7	8	201	500	CFRP	0.33	227	3800
	RC-4	270	1200	75.3	8	201	500	CFRP	0.33	227	3800

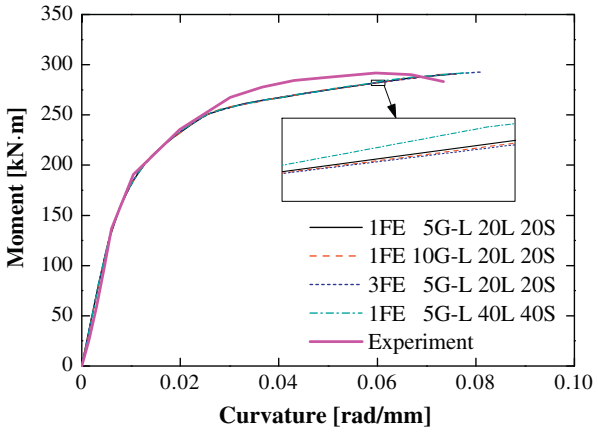

Fig. 3. Convergence analysis results: moment–curvature response of specimen ST3NT in [44].

3.2. Finite element model validation for columns subjected to concentric axial loading

In this section, the performance of the adopted frame FE was evaluated through a comparison between the experimentally measured and the numerically predicted load-carrying capacity and axial strain (i.e., axial displacement of the load application point divided by the specimen's length) at peak strength of the columns included in the experimental database for concentric axial loading (see Table 1). The geometric properties of the specimens and mechanical properties of the materials were taken from the literature [45–51]. The considered database contains specimens with a wide range of heights L (from 320 mm to 2000 mm), cross-section diameters d (from 160 mm to 508 mm), unconfined concrete compressive strength f'^2_{co} (from 25.93 MPa to 61.81 MPa), longitudinal steel reinforcement areas $A_s = n_b \cdot A_b$ (from 452 mm^2 to 3040 mm^2), and yield strength f_y (from 391 MPa to 620 MPa). The experimental database used in this study considers also a wide variety of FRP reinforcement configurations, with three materials (carbon FRP, glass FRP, and hybrid FRP), FRP material jacket thickness t_f varying in the range 0.176–3 mm, elastic modulus E_f varying in the range 19.1–241 GPa, and tensile strength f_j varying in the range 330–3937 MPa.

Table 3 presents the comparison between experimental results and numerical simulations of the load-carrying capacity and axial strain at peak strength for the reference RC columns (i.e., for the RC columns without FRP retrofit) subjected to concentric axial loading. The accuracy of the numerical model is investigated by using the ratio of the numerically simulated and experimentally measured load-carrying capacity, $R = P_{FE}/P_{exp}$ (where P_{FE} and P_{exp} = maximum axial load numerically predicted and experimentally measured, respectively), and axial strain at peak strength, $S = \varepsilon_{FE}/\varepsilon_{exp}$ (where ε_{FE} and ε_{exp} = axial strain at peak strength numerically predicted and experimentally measured, respectively). The agreement in terms of load-carrying capacity between experimental results and numerical simulations is excellent, with $\mu_R = 1.05$ (where μ_R = mean value of R) and $COV_R = 0.06$ (where COV_R = coefficient of variation of R). The agreement in terms of axial strain at peak strength between experimental results and numerical simulations is also very good, with $\mu_S = 0.94$ (where μ_S = mean value of S) and $COV_S = 0.08$ (where COV_S = coefficient of variation of S). These results are consistent with similar results reported in the existing literature [52,53].

Table 4 compares the experimentally measured and numerically simulated values of the load-carrying capacity and axial strain at peak strength of the selected FRP-confined RC columns subjected to concentric axial loads. The numerical simulations were performed using both the SM and the SZM models.

It is noteworthy that, for the concentric axial load case, the adopted FE model correctly identifies the failure mode of the FRP-confined RC specimens as FRP rupture. In particular, the SM model for the confined concrete tracks the value of the hoop strain during the entire loading procedure and identifies the concrete and specimen failure when the hoop strain is larger than or equal to the FRP failure strain. In this case, the statistics of both R and S (i.e., mean, standard deviation, coefficient of variation, and minimum and maximum values) are provided for both SM and SZM models. These statistics show that both models provide excellent results in terms of load-carrying capacity, with the SZM model ($\mu_{R_{SZM}} = 1.00$ and $\sigma_{R_{SZM}} = 0.07$) providing results that are slightly better than the SM model ($\mu_{R_{SM}} = 1.07$ and $\sigma_{R_{SM}} = 0.09$). The FE analyses performed using both material constitutive models overestimate the experimentally measured strain at peak strength, with the SM model ($\mu_{S_{SM}} = 1.23$ and $\sigma_{S_{SM}} = 0.31$) performing better than the SZM model ($\mu_{S_{SZM}} = 1.66$ and $\sigma_{S_{SZM}} = 0.56$). This overestimation is most likely due to the use in this study of the FRP ultimate strains

Table 3
Comparison between experimental results and numerical simulations for reference RC columns subjected to concentric axial loading: axial load-carrying capacity and strain at peak strength.

Ref.	ID	Maximum axial load (kN)			Axial strain at peak strength (mm/m)		
		Exp.	FE	*R*	Exp.	FE	*S*
[46]	00-LS320-3	3130	3709	1.18	2.38	2.36	0.99
[47]	C1	6648	6618	0.99	2.60	2.21	0.85
[48]	K1	4685	4705	1.00	2.80	2.80	1.00
[49]	C4NP0C	2930	2845	0.97	2.20	2.29	1.04
	C4MP0C	3917	4205	1.07	3.10	2.63	0.85
[50]	I.RCC.0L	594	624	1.05	3.77	3.87	1.03
	II.RCC.0L	1171	1210	1.03	3.02	2.53	0.84
	III.RCC.0L	1267	1341	1.06	2.69	2.53	0.94
[51]	C30	1917	2058	1.07	2.70	2.53	0.94
			Mean	St. Dev.	COV	Min.	Max.
	Max. axial load		1.05	0.06	0.06	0.97	1.18
	Axial strain at peak strength		0.94	0.08	0.08	0.84	1.04

directly reported in the references, i.e., no efficiency factors were applied to account for the fact that the FRP hoop strain at failure is usually smaller than the ultimate strain of FRP coupons obtained from axial tests [9,38,39]. In fact, the information provided in the considered references was generally insufficient to determine how the reported FRP ultimate strains were obtained (e.g., values given by the producer, or experimentally measured through axial testing of FRP coupons by the authors of the tests).

Fig. 4a and b graphically reproduce the results relative to the load-carrying capacity and axial strain at peak strength, respectively (see Tables 3 and 4). The insets of these figures depict loading and displacement for the concentric axial loading case. These two figures have the experimentally measured values on the vertical axis and the FE predictions on the horizontal axis. The dashed line on the main diagonal corresponds to perfect agreement between experimental values and numerical simulations, i.e., $R = 1.00$ and $S = 1.00$ for Fig. 4a and b, respectively. These results suggest that, for the specimen sizes considered here, the accuracy of the adopted frame FE in predicting the load-carrying capacity is not affected by scale effects. In addition, it is observed that the FE models employed in this study can predict with good accuracy the axial strain at peak strength for RC columns that are not confined with FRP, whereas they overestimated the axial strain at peak strength for RC columns confined with FRP, particularly for larger values of the strains. As previously explained, this overestimation is most likely due to the difference between the FRP hoop strain at failure and the ultimate strains obtained through axial testing of FRP.

3.3. Finite element model validation for columns subjected to eccentric axial loading

The performance of the newly developed frame FE was also evaluated through a comparison between the experimentally measured and the numerically predicted load-carrying capacity of the columns included in the experimental database and subjected to eccentric axial loading (see Table 2). The geometric properties of the specimens and mechanical properties of the materials are taken from experimental information provided in the literature [4,19,44,54–56]. The considered database contains specimens with a wide range of heights L (from 1200 mm to 3658 mm), cross-section diameters d (from 270 mm to 610 mm), unconfined compressive strength of concrete f'_{co} (from 34.45 MPa to 90.1 MPa), longitudinal steel reinforcement areas A_s (from 1608 mm^2 to 7384 mm^2) and yield strength f_y (from 303 MPa to 500 MPa), as well as a wide variety of FRP reinforcement configurations, FRP material jacket thickness t_f varying in the range 0.33–6.3 mm, elastic modulus E_f varying in the range 18.6–227 GPa, and FRP tensile strength f_j varying in the range 400–3800 MPa. The axial load ratio P/P_0 (where P = applied axial load, and $P_0 = f'_{co} \cdot A_g$, A_g = cross-section gross area) are given in Tables 5 and 6 and vary between 0.15 and 0.54. It is noted here that most of the specimens in [56] are made with high-strength concrete. However, the SM and SZM models were developed for normal-strength concrete and further research is needed to validate their use to model FRP-confined high-strength concrete. Since the adopted frame FE does not model shear failure, this study considers only specimens with a ratio L/d between the shear span length, L, and the diameter, d, larger than 3.0, in order to avoid specimens failing in shear. In addition, the selected experimental database considers only columns strengthened via FRP confinement (i.e., with FRP fibers oriented orthogonally to the column axis); thus, it excludes specimens retrofitted in flexure or in flexure-confinement (i.e., with FRP fibers oriented not orthogonally to the column axis). Research is ongoing to combine the frame FE proposed here with a frame FE previously developed by the second author to model RC elements that are flexurally-retrofitted with externally-bonded FRP [57]. The combination of these two frame FEs into a single nonlinear frame FE could be useful to model RC columns that are retrofitted with externally-bonded FRP in both flexure and confinement.

Table 5 presents the comparison between experimental results and numerical simulations of the load-carrying capacity for the reference RC columns (i.e., without FRP retrofit) under eccentric axial loading. The accuracy of the numerical model is investigated by using the ratio of the numerically simulated and experimentally measured load-carrying capacity, $R = F_{FE}/F_{exp}$ (where F_{FE} and F_{exp} = maximum lateral load numerically predicted and experimentally measured, respectively). The agreement in terms of load-carrying capacity between experimental results and numerical simulations is excellent, with $\mu_R = 1.02$ and $COV_R = 0.04$.

Table 6 compares the experimentally measured and numerically simulated values of the load-carrying capacities (in terms of maximum lateral load) of the selected FRP-confined RC columns subjected to eccentric axial loads. The numerical simulations were performed using both the SM and the SZM models. The statistics of R (i.e., mean, standard deviation, coefficient of variation, and minimum and maximum values) are provided for both models. These statistics show that both models provide excellent results in terms of load-carrying capacity (i.e., $\mu_{R_{SM}} = 1.02$ and $\sigma_{R_{SM}} = 0.06$ for the SM model, and $\mu_{R_{SZM}} = 1.00$ and $\sigma_{R_{SZM}} = 0.05$ for the SZM model, respectively).

Fig. 5 graphically reproduces the results relative to the load-carrying capacities for the column specimens subjected to eccentric axial load, which are provided in Tables 5 and 6. The inset of this figure also depicts loading and displacement for the eccentric axial loading case. The result indicates that, for all sizes of the specimens

Table 4
Comparison between experimental results and numerical simulations for FRP-confined RC columns subjected to concentric axial loading: axial load-carrying capacity and strain at peak strength.

Ref.	ID	Maximum axial load (kN)					Axial strain at peak strength (mm/m)				
		Exp.	SM	R_{SM}	SZM	R_{SZM}	Exp	SM	S_{SM}	SZM	S_{SZM}
[45]	C01-L0-20	4370	5202	1.19	4911	1.12	8.90	19.16	2.15	22.05	2.48
	C01-L0-26	5903	6905	1.17	6070	1.03	17.30	25.72	1.49	29.86	1.73
[46]	G01-L0-9	3895	4439	1.14	4570	1.17	7.39	10.83	1.46	17.50	2.37
	G01-L0-13	5500	6091	1.11	5784	1.05	12.51	21.32	1.70	24.93	1.99
[47]	C2	7479	7114	0.95	7797	1.04	8.80	7.65	0.87	7.27	0.83
	C3	7884	7139	0.91	8025	1.02	9.50	8.20	0.86	8.50	0.89
	C4	10134	8118	0.80	8991	0.89	11.60	23.14	1.99	12.02	1.04
[48]	K2	7460	7745	1.04	7115	0.95	11.1	11.3	1.02	15.70	1.41
	K3	7490	7590	1.01	7311	0.98	4.30	4.25	0.99	8.25	1.92
	K4	7580	7777	1.03	7510	0.99	6.90	8.2	1.19	15.00	2.17
	K5	5325	5458	1.02	5558	1.04	3.80	5.8	1.53	4.80	1.26
	K8	6230	6665	1.07	6333	1.02	5.90	6	1.02	8.8	1.49
[49]	A5NP2C	3326	3360	1.01	3231	0.97	6.30	6.75	1.07	8.75	1.39
	C4NP2C	3704	3809	1.03	3504	0.95	7.70	8.25	1.07	10.50	1.36
	C4NP4C	5468	5675	1.04	4866	0.89	20.80	22	1.06	22.75	1.09
	B4NP2C	4182	4255	1.02	4065	0.97	13.6	14.25	1.05	16.25	1.19
	C4MP2C	5434	5422	1.00	4994	0.92	8.80	10.75	1.22	14.75	1.67
[50]	I.RCC.1L	1003	1128	1.12	1129	1.12	15.34	15.94	1.04	18.75	1.22
	I.RCC.3L	1435	1595	1.11	1544	1.08	22.98	24.25	1.05	23.44	1.02
	II.RCC.1L	1558	1809	1.16	1594	1.02	8.36	8.75	1.05	20.62	2.47
	II.RCC.3L	2019	2561	1.27	2049	1.01	13.58	15.25	1.12	25.63	1.89
	III.RCC.1L	1532	1709	1.12	1586	1.03	3.75	4.53	1.21	11.25	3
	III.RCC.3L	1906	2164	1.14	1892	0.99	6.18	7.81	1.26	15.47	2.50
[51]	C10	1485	1670	1.12	1381	0.93	13.10	16.93	1.29	25.73	1.96
	C41	2767	3065	1.11	2804	1.01	9.10	11.73	1.29	17.60	1.93
	C34	3742	4033	1.08	3463	0.93	15.50	17.6	1.14	24.93	1.61
	C43	3967	4515	1.14	3700	0.93	16.60	18.4	1.11	23.47	1.41
	C44	4828	5363	1.11	4481	0.93	22.50	26.4	1.17	28.67	1.27
					Mean	St. Dev.		COV	Min.	Max.	
	Max. axial load (SM model)				1.07	0.09		0.09	0.80	1.27	
	Axial strain at peak strength (SM model)				1.23	0.31		0.25	0.86	2.15	
	Max. axial load (SZM model)				1.00	0.07		0.07	0.89	1.17	
	Axial strain at peak strength (SZM model)				1.66	0.56		0.34	0.83	3.00	

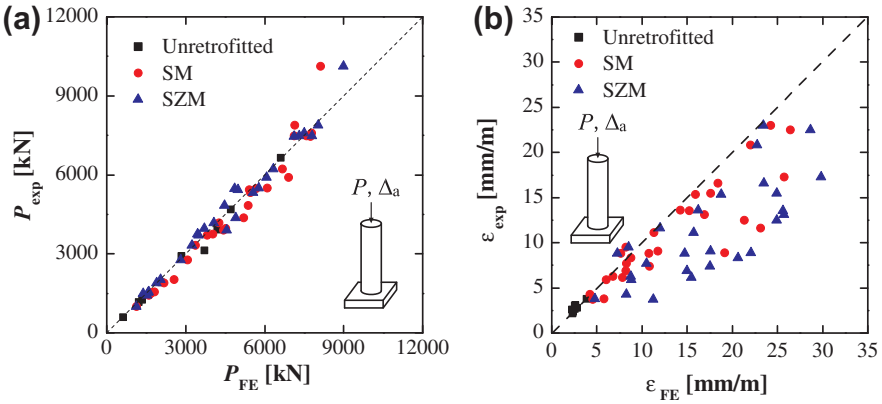

Fig. 4. Comparison between experimental and numerical results for columns subjected to concentric axial loading: (a) ultimate load-carrying capacity, and (b) strain at peak strength.

considered here, the FE models employed in this study can accurately predict the load-carrying capacity for both reference columns and FRP-confined RC columns.

It is noteworthy that the frame FE developed in this research automatically accounts for the different confining conditions experienced by different portions of the same cross-section under eccentric axial load conditions. In fact, while the same constitutive models are used for all concrete fibers in each cross-section under any type of loading condition, the two FRP-confined concrete material models adopted in this study account for the different confinement levels corresponding to different axial strain levels. In particular, the SM model accounts for varying confinement in a direct way by computing iteratively through equilibrium the concrete lateral strain and the corresponding FRP confinement pressure; whereas the SZM accounts for varying confinement indirectly through fitting to experimental results of the relation between axial strain and FRP confinement pressure. Thus, the adopted frame FE can also be used to predict the confinement

Table 5
Comparison between experimental results and numerical simulations for reference RC columns subjected to eccentric axial loading: lateral load-carrying capacity.

Ref.	ID	Axial load ratio P/P_0	Maximum lateral load (kN)		
			Exp.	FE	R
[54,19]	As-built	0.18	64	64.1	1.00
[4]	As-built	0.18	208	226	1.09
[44]	S-2NT	0.27	133	136.7	1.03
	S-3NT	0.54	126	130.6	1.04
	S-4NT	0.27	135	133.3	0.99
[55]	BR-C8	0.15	210	208.5	0.99
	Mean	St. Dev.	COV	Min.	Max.
Max. lateral load	1.02	0.04	0.04	0.99	1.09

Table 6
Comparison between experimental results and numerical simulations for FRP-confined RC columns subjected to eccentric axial loading: lateral load-carrying capacity.

Ref.	ID	Axial load ratio P/P_0	Maximum lateral load (kN)				
			Exp.	SM	R_{SM}	SZM	R_{SZM}
[54,19]	Upgraded	0.18	84	87.5	1.04	84.7	1.01
[4]	#1	0.18	272	297	1.09	290	1.07
	#2	0.18	310	302	0.97	293	0.95
[44]	ST-2NT	0.54	203	204.1	1.01	200.7	0.99
	ST-3NT	0.54	199	210.2	1.06	215	1.08
	ST-4NT	0.27	185	175.5	0.95	182.3	0.99
	ST-5NT	0.27	179	176.2	0.98	176.9	0.99
[55]	BR-C8-1	0.15	256	259	1.01	252	0.98
	BR-C8-2	0.15	263	244.5	0.93	242	0.92
[56]	RC-1	0.31	101	114	1.13	105	1.04
	RC-2	0.34	86	95	1.10	90.5	1.05
	RC-3	0.47	84	85.8	1.02	80.6	0.96
	RC-4	0.34	153	158	1.03	163	1.07
			Mean	St. Dev.	COV	Min.	Max.
	Max. lateral load (SM model)		1.02	0.06	0.06	0.95	1.13
	Max. lateral load (SZM model)		1.00	0.05	0.05	0.92	1.08

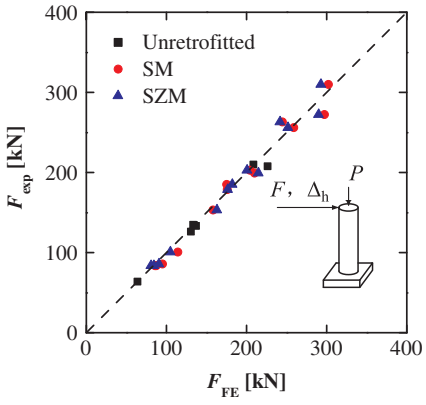

Fig. 5. Comparison between experimental and numerical results for columns subjected to eccentric axial loading: maximum lateral force.

efficiency of a given FRP confinement configuration under different loading conditions.

3.4. Comparison of force–displacement response

The accuracy of the adopted frame FE was also investigated through a comparison between the experimentally measured and the numerically predicted force–displacement response of the FRP-confined circular RC columns included in the experimental database considered in this study. Due to space constraints, this section describes in detail the force–displacement results corresponding to (1) the specimens identified as C4NP0C (unconfined specimen) and B4NP2C (FRP-confined specimen) in [49], as representative of columns subjected to concentric axial loading; and (2) the specimens identified as "as-built" (unconfined specimen) and "upgraded" (FRP-confined specimen) in [19] (in which the monotonic envelopes of the cyclic tests presented in [54] were reported), as representative of columns subjected to eccentric axial loading. It is noteworthy that the results corresponding to the other specimens considered in this study are similar to the select results presented in this section, as indicated by the results presented in Tables 4 and 6.

Fig. 6a plots the axial force–displacement response for the unretrofitted RC column (C4NP0C) and the FRP-confined RC column (B4NP2C) subjected to concentric axial loads. The thick lines correspond to the results for the C4NP0C specimen, whereas the thin lines correspond to the results for the B4NP2C specimen.

For the unretrofitted column, the agreement between numerical simulations and experimental records is excellent up to the peak strength (i.e., the numerical results capture well the initial stiffness, the stiffness degradation, and the peak strength of the specimen, with $R = 0.97$ and $S = 1.04$), and very good in the softening branch of the response, where the FE results slightly overestimate the post-peak residual strength of the column. It is noteworthy that the experimental axial force–displacement response of RC columns after the peak strength is usually affected by significant uncertainties and, thus, large discrepancies can be expected not only between numerical and experimental results, but also between different experimental tests performed on

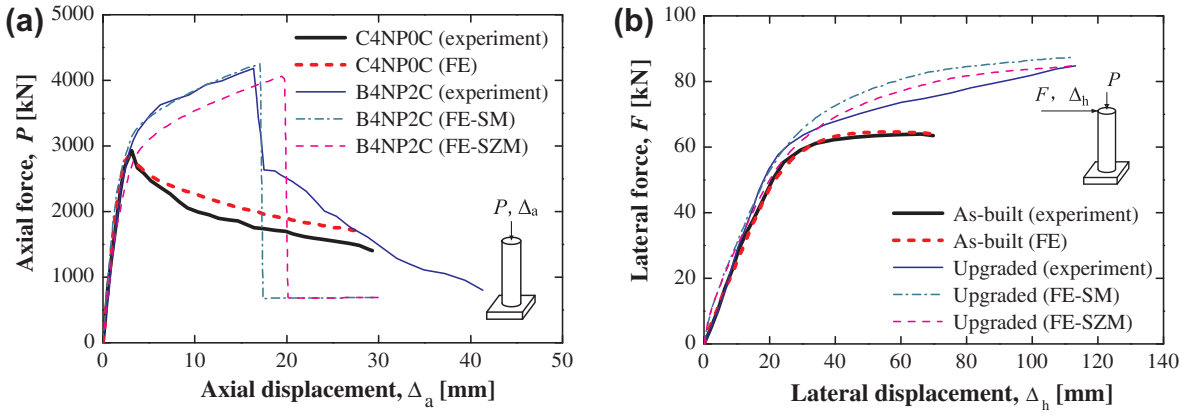

Fig. 6. Comparison between experimental and numerical results: (a) axial force–displacement response for concentric axial loading, and (b) lateral force–displacement response for eccentric axial loading.

equally-built specimens. These results are consistent with the results reported in [52]. For the FRP-confined RC column, the SM model provided results that are in excellent agreement with the experimental data in terms of initial stiffness, force at the yield point, post-yielding stiffness, peak strength, and displacement at the peak strength of the specimen. The SZM appeared to (1) underestimate by a very small amount the force at the yield point, (2) accurately capture the post-yielding stiffness and the peak strength, and (3) overestimate the displacement at the peak strength of the FRP-confined specimen. As expected, some discrepancies can be observed between the experimentally recorded and numerically simulated response of the specimens after the peak strength was achieved. This disagreement between experimental and numerical results may be due to the fact that, in the FE models, the FRP confinement fails along the entire length of the column during a single load step; whereas, in the experimental test, the FRP confinement may have failed locally at different locations for different values of the imposed axial displacement. However, this disagreement is neither a theoretical nor a practical limitation of the two models considered in this study due to the following considerations: (1) the post-peak response of FRP-confined RC columns is affected by significant uncertainties, the effects of which can be evaluated only by using probabilistic structural models; and (2) in real-world applications, FRP-confined RC columns are rarely loaded axially in displacement control. In addition, it is noteworthy that both the SM and SZM models identify the same residual strength after peak-strength for the column. The capability of these models to identify the column's residual strength after failure can be useful in the analysis of large structural systems, for which the failure of a single structural element may not correspond to the complete collapse of the structural system. Similar results were obtained also for the other FRP-confined RC columns subjected to concentric axial load and considered in this study.

These results confirm those presented in Tables 3 and 4 in terms of axial load-carrying capacity and strain at peak strength of the specimens. In addition, they suggest that the SM model can capture very well the initial stiffness of the column specimens, whereas the SZM slightly underestimates the initial stiffness of the column specimens. Both SM and SZM models capture the stiffness degradation before the peak strength and correctly identify the failure mode of FRP-confined RC columns subjected to concentric axial load as FRP rupture along the hoop direction.

Fig. 6b plots the lateral force–displacement response for the reference column ("as-built") and the FRP-confined RC column ("upgraded") subjected to eccentric axial load. The thick and thin lines correspond to the results for the "as-built" and the "upgraded" specimen, respectively. In this case, the agreement between numerical simulations and experimental records is excellent for both the reference column ($R = 1.00$) and the FRP-confined RC column ($R_{SM} = 1.04$ and $R_{SZM} = 1.01$). The SM model slightly overestimated the lateral force after yielding and the peak strength, whereas the SZM model slightly underestimated the stiffness of the specimen after the initial cracking of the concrete. The results presented here show that the adopted frame FE is able to accurately predict not only the peak strength of FRP-confined RC columns, but also their nonlinear force–displacement response under different loading conditions. This accuracy is achieved at a low computational cost, by using a very small number of FEs (only one in this case) to discretize the RC columns.

4. Conclusions

This paper presents a simple and efficient frame FE, which is able to accurately simulate the nonlinear response of circular RC columns confined with externally-bonded FRP. This frame FE uses a force-based formulation and a fiber-section discretization. Advanced material constitutive models are adopted to describe the nonlinear stress–strain behavior of steel, unconfined concrete, steel-confined concrete, and FRP-confined concrete.

The presented frame FE is used to predict the ultimate load-carrying capacity of FRP-confined RC columns subjected to concentric axial load (i.e., variable axial load only) and eccentric axial load (i.e., constant axial load and variable lateral load). Numerical simulations and experimental results are compared based on data available in the literature. The numerical simulation results are in excellent agreement with the experimental measurements in terms of peak strength and force–displacement responses.

The outstanding features of this frame FE are its simplicity, computational efficiency, and accuracy in predicting the structural behavior of circular RC columns confined with FRP even when a very coarse FE discretization is used to model a structural component. The major contribution of this study is the combination and implementation of existing modeling tools into a nonlinear frame FE that represents a step toward enabling the accurate and computationally efficient modeling of real-world full-scale structures with FRP-confined RC columns. Indeed, the major benefits of the adopted frame FE are achieved in the nonlinear FE analysis of real-world large-scale structures, for which the focus is on the global structural response rather than on the local behavior at the single member or material levels. Further studies are ongoing to extend the presented frame FE to analysis of columns with rectangular cross-section, with shear span over diameter ratio $L/d \leqslant 3$, and with local buckling of the longitudinal reinforcement.

Acknowledgements

The authors grateful acknowledge partial support of this research by the Louisiana Board of Regents (LA BoR) through the Louisiana Board of Regents Research and Development Program, Research Competitiveness (RCS) subprogram, under Award No. LESQSF (2010-13)-RD-A-01. Any opinions, findings, conclusions, or recommendations expressed in this publication are those of the writers and do not necessarily reflect the views of the sponsor.

References

[1] Van Den Einde L, Zhao L, Seible F. Use of FRP composites in civil structural applications. Constr Build Mater 2003;17(6–7):389–403.
[2] Bank LC. Composites for construction: structural design with FRP materials. Hoboken, NJ, USA: Wiley; 2007.
[3] Nanni A, Bradford NM. FRP jacked concrete under uniaxial compression. Constr Build Mater 1995;9(2):115–24.
[4] Seible F, Priestley MJN, Hegemier GA, Innamorato D. Seismic retrofit of RC columns with continuous carbon fiber jacket. J Compos Constr 1997;1(2):52–62.
[5] Bakis CE, Bank LC, Brown VL, Cosenza E, Davalos JF, Lesko JJ, Rizkalla SH, Triantafillou TC. Fiber-reinforced polymer composites for construction-State-of-the-art review. J Compos Constr 2002;6(2):73–8.
[6] Flaga K. Advances in materials applied in civil engineering. J Mater Process Technol 2000;106(1):173–83.
[7] Mertz DR, Chajes MJ, Gillespie JW, Kukich DS, Sabol SA, Hawkins NM, et al. Application of fiber reinforced polymer composites to the highway infrastructure. NCHRP Report 503, Transportation Research Board: Washington, DC, USA; 2003.
[8] Motavalli M, Czaderski C. FRP composites for retrofitting of existing civil structures in Europe: state-of-the art review. In: Composites and polycon, American composites manufactures association, Tampa, FL, USA; 2007.
[9] Lam L, Teng JG. Design-oriented stress–strain model for FRP-confined concrete. Constr Build Mater 2003;17(6–7):471–89.
[10] Fardis MN, Khalili HH. FRP-encased concrete as a structural material. Mag Concr Res 1982;34(121):191–202.
[11] Karbhari VM, Gao Y. Composite jacketed concrete under uniaxial compression-verification of simple design equations. J Mater Civ Eng 1997;9(4):185–93.
[12] Samaan M, Mirmiran A, Shahawy M. Model of concrete confined by fiber composites. J Struct Eng 1998;124(9):1025–31.
[13] Toutanji HA. Stress–strain characteristics of concrete columns externally confined with advanced fiber composite sheets. ACI Mater J 1999;96(3):397–404.
[14] Xiao Y, Wu H. Compressive behavior of concrete confined by carbon fiber composite jackets. J Mater Civ Eng 2000;12(2):139–46.
[15] Mirmiran A, Shahawy M. A new concrete-filled hollow FRP composite column. Composites: Part B 1996;27B(3–4):263–8.
[16] Spoelstra MR, Monti G. FRP-confined concrete model. J Compos Constr 1999;3(3):143–50.
[17] Fam AZ, Rizkalla SH. Confinement model for axially loaded concrete confined by circular fiber-reinforced polymer tubes. ACI Struct J 2001;98(4):451–61.
[18] Shao Y, Zhu Z, Mirmiran A. Cyclic modeling of FRP-confined concrete with improved ductility. Cement Concr Compos 2006;28(10):959–68.
[19] Monti G, Nistico N, Santini S. Design of FRP jackets for upgrade of circular bridge piers. J Compos Constr 2001;5(2):94–101.
[20] Yuan XF, Xia SH, Lam L, Smith ST. Analysis and behavior of FRP-confined short concrete columns subjected to eccentric loading. J Zhejiang Univ Sci A 2007;9(1):38–49.
[21] Mirmiran A, Zagers K, Yuan WQ. Nonlinear finite element modeling of concrete confined by fiber composites. Finite Element Anal Des 2000;35(1):79–96.
[22] Karabinis AI, Rousakis TC, Manolitsi GE. 3D finite-element analysis of substandard RC columns strengthened by fiber-reinforced polymer sheets. J Compos Constr 2008;12(5):531–40.
[23] Yu T, Teng JG, Wong YL, Dong SL. Finite element modeling of confined concrete-II: Plastic-damage model. Eng Struct 2010;32(3):680–91.
[24] Parvin A, Wang W. Concrete columns confined by fiber composite wraps under combined axial and cyclic lateral loads. Compos Struct 2002;58(4):539–49.
[25] Malvar LJ, Morrill KB, Crawford JE. Numerical modeling of concrete confined by fiber-reinforced composites. J Compos Constr 2004;8(4):315–22.
[26] Varma RK, Barros JAO, Sena-Cruz JM. Numerical model for CFRP confined concrete elements subject to monotonic and cyclic loadings. Composites: Part B 2009;40(8):766–75.
[27] Binici B, Mosalam KM. Analysis of reinforced concrete columns retrofitted with fiber reinforced polymer lamina. Composites: Part B 2007;38(2):265–76.
[28] Spacone E, Filippou FC, Taucer FF. Fiber beam-column element for nonlinear analysis of R/C frames. Part I: Formulation. Earthq Eng Struct Dynam 1996;25(7):11–25.
[29] Neuenhofer A, Filippou FC. Evaluation of nonlinear frame finite-element models. J Struct Eng 1997;123(7):958–66.
[30] Menegotto M, Pinto PE. Method of analysis for cyclically loaded reinforced concrete plane frames including changes in geometry and nonelastic behavior of elements under combined normal force and bending. In: Proceedings, IABSE symposium on resistance and ultimate deformability of structures acted on by well-defined repeated loads, Lisbon, Portugal; 1973.
[31] Filippou FC, Popov EP, Bertero VV. Effects of bond deterioration on hysteretic behavior of reinforced concrete joints. Report EERC 83-19, Earthquake Engineering Research Center, University of California, Berkeley, California, USA; 1983.
[32] Monti G, Nuti C. Non-linear cyclic behavior of reinforcing bars including buckling. J Struct Eng 1992;118(12):3268–84.
[33] Balan TA, Filippou FC, Popov EP. Constitutive model for 3D cyclic analysis of concrete structures. J Eng Mech 1997;123(2):143–53.
[34] Balan TA, Spacone E, Kwon MA. 3D hypoplastic model for cyclic analysis of concrete structures. Eng Struct 2001;23(4):333–42.
[35] Kwon M, Spacone E. Three dimensional finite element analyses of reinforced concrete columns. Comput Struct 2002;80(2):199–212.
[36] Mander JB, Priestley MJN, Park R. Theoretical stress–strain model for confined concrete. J Struct Eng 1988;114(8):1804–26.
[37] Monti G, Barbato M. Fiber-section FE of FRP-strengthened RC beam in flexure, shear and confinement. In: Proceedings, 6th international symposium on fibre-reinforced polymer (FRP) reinforcement for concrete structures, July 8–10, 2003, National University of Singapore, Singapore, Singapore; 2003.
[38] American Concrete Institute (ACI). Guide for the design and construction of externally bonded FRP systems for strengthening concrete structures (ACI 4402R-08). MI, USA: Farmington Hills; 2008.
[39] Rocca S, Galati N, Nanni A. Interaction diagram methodology for design of FRP-confined reinforced concrete columns. Constr Build Mater 2009;23(4):1508–20.
[40] De Caso y Basalo F, Matta F, Nanni A. Novel test method for ultimate hoop strain characterization in FRP jackets. J Mater Civ Eng 2011;23(12):1633–41.
[41] Filippou FC, Constantinides M. EDEASLab getting started guide and simulation examples, Technical Report NEESgrid. vol. 22; 2004.
[42] MathWorks Inc. Matlab – high performance numeric computation and visualization software. User's guide, Natick, MA, USA; 1997.
[43] Bathe KJ. Finite element procedures. Englewood Cliffs, NJ, USA: Prentice-Hall; 1995.
[44] Sheikh SA, Yau G. Seismic behavior of concrete columns confined with steel and fiber-reinforced polymers. ACI Struct J 2002;99(1):72–80.
[45] Cairns SW. Circular concrete columns externally reinforced with pre-fabricated carbon polymer shells. Master Thesis, Department of Civil Engineering, University of Toronto, Toronto, Canada; 2001.
[46] Jaffry SAD. Concrete-filled glass fiber reinforced polymer (GFRP) shells under concentric compression. Master Thesis, Department of Civil Engineering, University of Toronto, Toronto, Canada; 2001.
[47] Pessiki S, Harries KA, Kestner JT, Sause R, Ricles JM. Axial behavior of reinforced concrete columns confined with FRP jackets. J Compos Constr 2001;5(4):237–45.
[48] Matthys S, Toutanji H, Taerwe L. Stress–strain behavior of large-scale circular columns confined with FRP composites. J Struct Eng 2006;132(1):123–33 [ASCE].
[49] Eid R, Roy N, Paultre P. Normal- and high-strength concrete circular elements wrapped with FRP composites. J Compos Constr 2009;13(2):113–24.
[50] Benzaid R, Mesbah H, Chikh NE. FRP-confined concrete cylinders: axial compression experiments and strength model. J Reinf Plast Compos 2010;29(16):2469–88.
[51] Chastre C, Silva MAG. Monotonic axial behavior and modelling of RC circular columns confined with CFRP. Eng Struct 2010;32(8):2268–77.
[52] Mander JB, Priestley MJN, Park R. Observed stress–strain behavior of confined concrete. J Struct Eng 1988;114(8):1827–49.
[53] Lee TH, Mosalam KM. Probabilistic fiber element modeling of reinforced concrete structures. Comput Struct 2004;82(27):2285–99.
[54] Saadatmanesh H, Ehsani MR, Jin L. Seismic strengthening of circular bridge pier models with fiber composites. ACI Struct J 1996;93(6):639–47.
[55] Elnabelsy G, Saatcioglu M. Design of FRP jackets for seismic retrofit of circular concrete columns. Emirates J Eng Res 2004;9(2):65–9.
[56] Ozbakkaloglu T, Saatcioglu M. Seismic behavior of high-strength concrete columns confined by fiber-reinforced polymer tubes. J Compos Constr 2006;10(6):538–49.
[57] Barbato M. Efficient finite element modelling of reinforced concrete beams retrofitted with fibre reinforced polymers. Comput Struct 2009;87(3–4):167–76.